

Improved model predictive current control for multi-mode four-switch buck–boost converter considering parameter mismatch

Yan Wu¹ | Wei Wang¹ | Fen Tang¹ | Xuezhi Wu¹ | Zhe Chen² | Long Jing¹ | Weige Zhang¹

¹School of Electrical Engineering, Beijing Jiaotong University, Beijing, China

²Department of Energy Technology, Aalborg University, Aalborg, Denmark

Correspondence

Fen Tang, Electrical Engineering Building, Beijing Jiaotong University, Beijing 100044, China.
Email: fent@bjtu.edu.cn

Funding information

Delta Power Electronics Science and Education Development Plan, Grant/Award Number: DREK2021005

Abstract

Four-switch Buck-Boost (FSBB) converter usually adopts multi-mode control methods in applications requiring both voltage step-up and step-down. Model predictive current control (MPCC) can improve the dynamic performance and simplify multi-mode switching control, but parameter mismatch will deteriorate its control performances. To this end, the theoretical steady-state error of MPCC caused by parameter mismatch is derived; the influence of parameter mismatch on the dynamic and steady-state performances is analyzed. Further, an improved MPCC strategy with the parameter disturbance observer (PDO) and dynamic adjustment block for the FSBB converter is presented. The PDO is developed to correct the prediction model and eliminate steady-state errors due to parameter mismatch. The dynamic adjustment block related to the tracking error can further avoid the dynamic performance degradation. Additionally, a load disturbance observer (LDO) is designed to improve the dynamic response to the unknown load variation. Then, multi-mode operation of the FSBB converter is realized with the proposed MPCC, which determines the operating mode according to the prediction results without extra mode detection. Finally, simulation and experimental results demonstrate that the proposed strategy can improve the dynamic and steady-state performances of MPCC with parameter mismatch and achieve multi-mode operation with high control performances.

1 | INTRODUCTION

The FSBB converter is a DC/DC converter with the same polarity of input and output voltage, which can achieve both voltage step-up and step-down [1, 2]. Furthermore, it can easily implement the functions of Buck, Boost, and Buck–Boost converters due to its circuit topology [3, 4]. These characteristics make the FSBB converter suitable for many low-power and high-power applications, such as consumer electronics, power supply, new energy power generation, energy storage systems, fuel cell systems etc. [5–7].

At present, the controllers of the FSBB converter are mainly designed with multi-mode control methods. The two-mode control method [8] is one of the simplest methods, where the

FSBB converter has the Buck and Boost modes. However, due to the limitation of the maximum and minimum duty cycles of actual switches, there is a control dead zone when the input voltage is close to the output voltage [9, 10]. To overcome this issue, some studies add extra operating modes for this operating condition [11–14]. A three-mode control scheme is proposed in [12], which has a Buck–Boost mode between the Buck and Boost modes. The method of overlapping the Buck and Boost modes by clamping the duty cycles of the switches on one arm of the FSBB converter when the input voltage approaches the output voltage is reported in [13] and [14], the voltage control is achieved by adjusting the duty cycles of the switches on another arm. These methods can avoid the control dead zone, but they may suffer from other problems.

This is an open access article under the terms of the [Creative Commons Attribution-NonCommercial-NoDerivs](#) License, which permits use and distribution in any medium, provided the original work is properly cited, the use is non-commercial and no modifications or adaptations are made.

© 2023 The Authors. *IET Power Electronics* published by John Wiley & Sons Ltd on behalf of The Institution of Engineering and Technology.

As the number of operating modes increases, the controller design becomes more complex. If the controller with the same parameters is used for different modes, the optimal control performance cannot be guaranteed for each mode due to their different circuit operating states. However, if separate controllers are used, extra mode detection is usually required for mode switching control; the required accuracy and speed of mode detection are high. Besides, the conventional multi-mode controllers usually adopt the linear control method, but it is difficult to obtain a good dynamic performance for high-power applications where a relatively low switching frequency is usually required [15]. Therefore, the multi-mode control with good performances still needs to be further investigated for the FSBB converter.

In recent years, some non-linear control methods have attracted increasing attention for power electronics due to the non-linear characteristic of the converters, such as model predictive control (MPC), fuzzy logic control, sliding mode control, adaptive control etc. [16, 17]. These methods have increasingly been used in DC/DC converters; they exhibit better control performances compared with the linear control methods. Among them, MPC has the advantages of fast dynamic response and intuitive control logic design; it can flexibly adjust the control logic according to the control needs [18, 19]. Many studies have begun to apply MPC to the DC/DC converters [20–24]. A cascaded voltage controller for the Boost converter is proposed in [22], using model predictive current control (MPCC) to replace the current loop in the conventional proportional-integral (PI) double-loop controller. An MPC-based voltage control strategy with a cost function is proposed in [23], which adopts an enumeration method to determine all the switch states. It has been shown to achieve good control effects on the single-input multi-output Buck converter. An MPCC method for the FSBB converter is presented in [24] that designs a cost function to determine the operation mode; it improves the control performance for multi-mode switching control. Combining the prediction mechanism of MPC with mode switching control can simplify the work of multi-mode switching control. But it is well known that MPC is a method based on the controlled object model, which makes it sensitive to parameter mismatch. This problem has not been fully investigated in the above studies. The prediction model of the converter is usually established based on the converter parameters. For the FSBB converter, the inductance and series resistance are the most important parameters for its prediction model. Unfortunately, they are often difficult to obtain accurate values by measurement when the converter is running, and may also vary with operating conditions. The parameter uncertainty and random disturbance will affect the accuracy of the prediction model, which may result in oscillations and control deviations [25, 26]. This problem can be solved by the online parameter identification [27], but accurate identification of multiple parameters is difficult to realize in practice due to the high requirement for the computing power of the controller.

To overcome the above issues, some improved MPC methods have been proposed. In the current controller based on

MPCC of the Boost converter designed in [15], an observer is designed to observe the change of the load as the basis for adjusting the current reference. This method improves the dynamic response to handle load disturbances, but does not yet solve the problem of parameter mismatch. In fact, the model deviations due to parameter mismatch can be estimated by various observers [28, 29] and the estimated results can be used to correct the prediction model. An offset-free composite MPC strategy for the Buck converter is presented in [30], where the voltage control is designed as a backward optimization problem. And for the unknown loads and the uncertainty of the system, a higher order sliding mode observer is designed and combined into the optimization problem. However, this method is complex; this problem will be further highlighted if applied to FSBB converters due to more operating modes. The deadbeat current predictive control is employed in the modular multilevel converter in [31]; it solves the inductance mismatch by identifying the inductance, but it ignores the influence of parasitic resistance. The above studies are effective in improving the control accuracy of MPC, but they mainly focus on eliminating steady-state errors; the impact on dynamic performance is insufficiently considered. In fact, the parameter mismatch can affect both the dynamic and steady-state control performances. Therefore, further research is still required to reduce the influence of parameter mismatch on the control performances of MPC.

This paper focuses on the control strategy of the FSBB converter for high-power applications with the relatively low switching frequency. Aiming at improving the dynamic and steady-state performances of MPCC with parameter mismatch and achieving multi-mode operation of the FSBB converter with high performances, an improved MPCC strategy for the FSBB converter is proposed. First, the steady-state error of MPCC caused by the inductance and series resistance mismatch of the FSBB converter is derived theoretically; the influence of parameter mismatch on MPCC is analyzed in detail. Then, an improved MPCC strategy with a parameter disturbance observer (PDO) and dynamic adjustment block is developed, which can eliminate the steady-state errors based on the estimated model deviation and retain a fast dynamic response with parameter mismatch. In addition, a load disturbance observer (LDO) is designed to improve the dynamic response to random load disturbances. Based on the proposed MPCC, the multi-mode switching control without extra mode detection of the FSBB converter is achieved. Finally, the proposed strategy is compared with the multi-mode control strategies using PI control and conventional MPCC strategy through the simulations and experiments.

This paper is organized as follows: Section 2 introduces the operating principle of the FSBB converter and the existing challenges. Section 3 analyzes the influence of parameter mismatch on MPCC. The details of the proposed strategy are presented in Section 4. Simulation and experimental results are given in Sections 5 and 6, respectively. Finally, Section 7 summarizes the work of this paper.

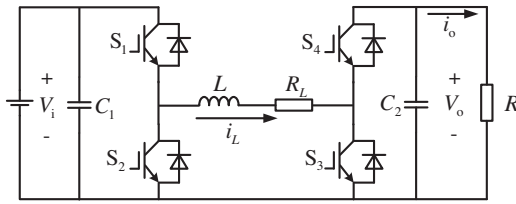


FIGURE 1 Topology of the FSBB converter. FSBB, four-switch buck-boost.

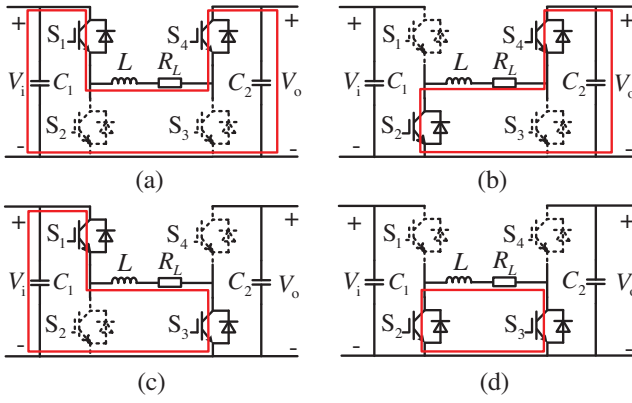


FIGURE 2 Circuit states of the FSBB converter. (a) State 1. (b) State 2. (c) State 3. (d) State 4

2 | OPERATIONAL PRINCIPLE OF FSBB CONVERTER

2.1 | Operation principle and mathematical model

The topology of the FSBB converter is shown in Figure 1, where S_1 to S_4 are power switches and their freewheeling diodes. S_1 to S_4 are all bidirectional and the energy flow of the converter can also be bidirectional. C_1 and C_2 represent the input and output capacitances, respectively. L is the inductor, R_L is the total equivalent series resistance of the inductor current path and R represents the load. V_i is the input voltage and V_o is the output voltage. The FSBB converter has four circuit states according to the on-off state of switches, as shown in Figure 2. The continuous conduction mode is considered and analyzed in this paper. For the application of the bidirectional FSBB converter, the analysis processes and conclusions for the forward and reverse energy flow are identical due to its symmetrical topology.

The FSBB converter circuit can be divided into two parts, S_1 and S_2 form a Buck unit, S_3 and S_4 form a Boost unit. As shown in Figure 2, the FSBB converter will work as a Buck converter when it switches between states 1 and 2. Similarly, the FSBB converter will work as a Boost converter when it switches between states 1 and 3. The inductor current flows only inside the converter in state 4, in order to simplify the multi-mode control, state 4 is not used as an effective circuit state in the following contents. In the ideal situation, the relationship of V_o

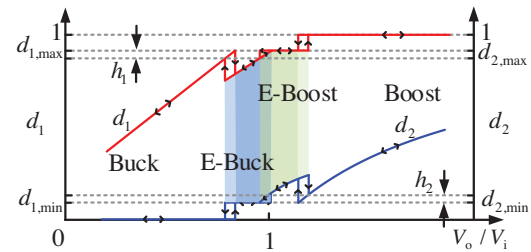


FIGURE 3 Schematic of the four-mode control with duty cycle hysteresis

and V_i can be expressed as

$$\frac{V_o}{V_i} = \frac{d_1}{1 - d_2} \quad (1)$$

where d_1 and d_2 are the duty cycles of S_1 and S_3 , respectively.

The average state model of the FSBB converter can be expressed as

$$\begin{cases} \frac{di_L(t)}{dt} = \frac{V_i(t)}{L} d_1(t) - \frac{i_L(t)R_L}{L} - \frac{V_o(t)}{L} [1 - d_2(t)] \\ \frac{dV_o(t)}{dt} = \frac{i_L(t)}{C_2} [1 - d_2(t)] - \frac{i_o(t)}{C_2} \end{cases} \quad (2)$$

2.2 | Multi-mode control method

In order to ensure that the FSBB converter can realize the voltage conversion without control dead zone in the whole operating range, multi-mode control methods are usually adopted [5, 12–14]. A four-mode control method is shown as Figure 3, where $d_{1,\max}$ and $d_{1,\min}$ are the maximum and minimum values of d_1 , respectively, $d_{2,\max}$ and $d_{2,\min}$ are the maximum and minimum values of d_2 , respectively. In general, $d_{1(2),\max} + d_{1(2),\min} = 1$. When V_i is significantly higher or lower than V_o , the FSBB converter operates in Buck or Boost mode. In the condition when V_i is close to V_o , the extended modes are adopted. The switching losses in the extended modes are more than those in the Buck or Boost mode due to the switch actions of S_1 to S_4 in each switching cycle. Hence, the operating range of the extended modes should be minimized under the condition of ensuring the elimination of dead zone. Meanwhile, in order to reduce the average inductor current, d_2 should be as small as possible and d_1 should be as large as possible [12]. Therefore, in the extended Buck (E-Buck) mode, the voltage step-down control is achieved by clamping d_2 to its minimum value and only adjusting d_1 . Similarly, in the extended Boost (E-Boost) mode, the voltage step-up control is achieved by clamping d_1 to its maximum value and only adjusting d_2 .

It is worth noting that the voltage gains at the mode boundary are approximately equal for the two adjacent operating modes. When the FSBB converter operates near the mode boundary, frequent mode switching is likely to occur, resulting in unstable

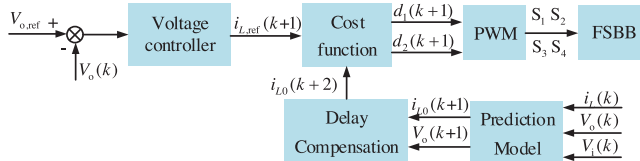


FIGURE 4 The control block diagram of MPCC. MPCC, model predictive current control.

output voltage. To avoid undesired mode switching as much as possible, the duty cycle hysteresis is added when the FSBB converter operates near the mode boundary as shown in Figure 3, where b_1 and b_2 are the hysteresis width.

2.3 | Existing challenges

Multi-mode control methods can effectively eliminate the control dead zone of the FSBB converter due to the duty cycle limitation of actual switches. However, it faces the problem of complex multi-mode controller design. In order to achieve smooth mode switching, the controller needs to have a better dynamic response. Among the conventional multi-mode controllers for the FSBB converter, the linear control like PI controller is most common, but it is difficult to obtain a good control performance on mode switching due to the lagging characteristic, especially in high-power applications where a relatively low switching frequency is required. Therefore, the multi-mode control method for the FSBB converter needs to be further optimized in terms of mode switching control and high performance.

Since MPCC has the characteristics of simple design and fast dynamic response, applying MPCC in multi-mode switching control of the FSBB converter can simplify the work of mode switching control and improve the dynamic response. However, there is also a possibility of parameter mismatch in the actual application of MPCC in the FSBB converter. This problem may reduce the dynamic and steady-state performances of MPCC. The existing studies on parameter mismatch mainly focus on the analysis and improvement of the steady-state performance, but the impact on the dynamic performance is still lacking of discussion and research. To fully utilize the advantages of MPCC, the influence of parameter mismatch and solutions need to be further analyzed and investigated.

3 | ANALYSIS OF THE INFLUENCE OF PARAMETER MISMATCH ON MPCC

The control block diagram of MPCC is shown as Figure 4.

From (2), the discrete-time state space model of the FSBB converter can be derived by the one-order forward Euler approximation method as shown in (3); it can be used as the prediction model of the FSBB converter.

$$\begin{cases} \mathbf{x}(k+1) = A\mathbf{x}(k) + B\mathbf{v}(k) \\ \mathbf{y}(k) = C\mathbf{x}(k) \end{cases} \quad (3)$$

$$A = \begin{bmatrix} 1 - \frac{R_L T_s}{L} & -\frac{T_s}{L}[1 - d_2(k)] \\ \frac{T_s}{C_2}[1 - d_2(k)] & 1 \end{bmatrix},$$

$$B = \begin{bmatrix} \frac{T_s}{L}d_1(k) & 0 \\ 0 & -\frac{T_s}{C_2} \end{bmatrix},$$

$$C = [1 \quad 0].$$

where T_s is the control cycle. $\mathbf{x}(k) = [i_L(k) \ V_o(k)]^T$, $\mathbf{y}(k) = i_L(k)$, $\mathbf{v}(k) = [V_i(k) \ i_o(k)]^T$, A , B and C are coefficient matrices.

In (3), when the FSBB converter operates in the Buck mode, $d_2(k) = 0$; when it operates in the E-Buck mode, $d_2(k) = d_{2,\min}$; when it operates in the E-Boost mode, $d_1(k) = d_{1,\max}$; and when it operates in the Boost mode, $d_1(k) = 1$.

It is worth noting that there is a one-step control delay from the calculation of the control commands to the update of the switch actions in the digital control, which may cause problems such as control deviation and even oscillation problems [31]. Thus, it is very necessary to compensate the control delay in actual applications of MPCC. In this paper, the control delay compensation is carried out by one step ahead prediction which has been discussed in [18]. When the sampling results $V_i(k)$, $V_o(k)$, $i_L(k)$ are obtained at the instant k , the system state $\mathbf{x}(k+1)$ at the instant $k+1$ can be predicted according to the prediction model. Based on this, the inductor current $i_{L0}(k+2)$ can be predicted. Then, it is used for the duty cycles calculation, so that the effects of the control delay can be reduced.

In order to reduce the computational burden of the controller, a single-step prediction horizon is adopted. The cost function of MPCC is defined as (4). By performing a derivative calculation on (4) that is shown in (5), the duty cycles of the next control cycle can be obtained.

$$J = [i_{L0}(k+2) - i_{L,\text{ref}}(k+1)]^2 \quad (4)$$

$$\frac{\partial J}{\partial d} = 0 \quad (5)$$

where d represents d_1 when the FSBB converter operates in the Buck or E-Buck mode, d represents d_2 in the E-Boost or Boost mode.

For the FSBB converter, the parameters that mainly affect the accuracy of the prediction model are the inductance and series resistance. Due to the influence of the temperature, operating time, magnetic saturation characteristic and the current through the converter, there are unavoidable deviations between the actual values and parameter values used in the prediction model. Hence, the influence of the inductance and series resistance mismatch needs to be focused and analyzed.

According to (3), the predicted inductor current and actual inductor current at the instants $k+1$ and $k+2$ can be derived as

$$\begin{cases} i_{L,0}(k+1) = \left(1 - \frac{R_{L,0}T_s}{L_0}\right)i_L(k) - \frac{[1 - d_2(k)]T_s}{L_0}V_o(k) \\ \quad + \frac{d_1(k)T_s}{L_0}V_i(k) \\ i_{L,0}(k+2) = \left(1 - \frac{R_{L,0}T_s}{L_0}\right)i_{L,0}(k+1) - \frac{[1 - d_2(k+1)]T_s}{L_0}V_o(k+1) \\ \quad + \frac{d_1(k+1)T_s}{L_0}V_i(k+1) \end{cases} \quad (6)$$

where L_0 and $R_{L,0}$ are the parameter values of inductance and series resistance used in the prediction model, respectively.

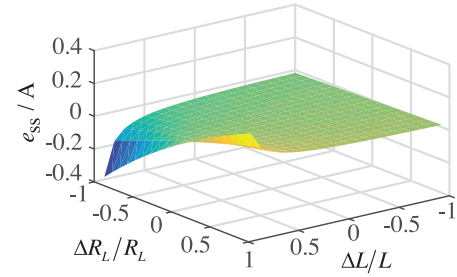


FIGURE 5 Influence trend of the parameter mismatch on the steady-state error

By performing $\tilde{\zeta}$ -transformation on (8), the discrete transfer function between the actual inductor current and its reference considering the delay compensation can be obtained as shown in (9). The discrete system is stable if all the system poles are within the unit circle in the $\tilde{\zeta}$ -plane.

$$\frac{i_L(\tilde{\zeta})}{i_{L,\text{ref}}(\tilde{\zeta})} = \frac{L^2\tilde{\zeta}}{LL_0\tilde{\zeta}^2 + (L_0R_L - LR_{L,0})T_s\tilde{\zeta} - \Delta LL_0 + (\Delta R_L L_0 + \Delta LR_{L,0})T_s - R_{L,0}\Delta R_L T_s^2} \quad (9)$$

$$\begin{cases} i_L(k+1) = \left(1 - \frac{R_L T_s}{L}\right)i_L(k) - \frac{[1 - d_2(k)]T_s}{L}V_o(k) \\ \quad + \frac{d_1(k)T_s}{L}V_i(k) \\ i_L(k+2) = \left(1 - \frac{R_L T_s}{L}\right)i_L(k+1) - \frac{[1 - d_2(k+1)]T_s}{L}V_o(k+1) \\ \quad + \frac{d_1(k+1)T_s}{L}V_i(k+1) \end{cases} \quad (7)$$

where L and R_L are the actual values of inductance and series resistance, respectively.

Ignoring the changes of V_i and V_o in the two adjacent sampling periods, that is, assuming $V_o(k+1) = V_o(k)$, $V_i(k+1) = V_i(k)$, the relationship between the actual inductor current and its reference can be derived as (8) by combining (5) to (7).

$$\begin{aligned} & Li_L(k+2) + \left(R_L T_s - \frac{LR_{L,0}T_s}{L_0}\right)i_L(k+1) \\ & - \left[\Delta L - \Delta R_L T_s - \frac{LR_{L,0}T_s}{L_0} + R_{L,0}T_s + \frac{R_{L,0}\Delta R_L T_s^2}{L_0}\right] \\ & i_L(k) = L_0 i_{L,\text{ref}}(k+1) \end{aligned} \quad (8)$$

where $\Delta L = L - L_0$, $\Delta R_L = R_L - R_{L,0}$.

The error $E(\tilde{\zeta})$ of MPCC can be expressed as

$$E(\tilde{\zeta}) = i_{L,\text{ref}}(\tilde{\zeta}) - i_L(\tilde{\zeta}). \quad (10)$$

According to the final value theorem of automatic control theory, when $i_{L,\text{ref}}(\tilde{\zeta})$ is a unit step action as shown in (11), the steady-state error of MPCC can be derived as shown in (12). Further, the influence trend of the parameter mismatch on the steady-state error can be depicted in Figure 5. It can be seen that the main factor affecting the steady-state error is the series resistance mismatch, $|e_{ss}|$ increases as the deviation $|\Delta R_L|$ increases. Moreover, when the series resistance is mismatched, $|e_{ss}|$ increases as the deviation ΔL increases.

$$i_{L,\text{ref}}(\tilde{\zeta}) = \frac{\tilde{\zeta} - 1}{\tilde{\zeta}} \quad (11)$$

$$e_{ss} = \lim_{z \rightarrow 1} (1 - z^{-1}) E(z) = \frac{2L_0\Delta R_L T_s - R_{L,0}\Delta R_L T_s^2}{L_0^2 + 2L_0\Delta R_L T_s - R_{L,0}\Delta R_L T_s^2} \quad (12)$$

The predicted inductor current change can be expressed as

$$\begin{aligned} & |i_{L,0}(k+1) - i_L(k)| \\ & = \left| \frac{V_i(k)d_1(k)T_s - R_{L,0}i_L(k)T_s - V_o(k)[1 - d_2(k)]T_s}{L_0} \right| \end{aligned} \quad (13)$$

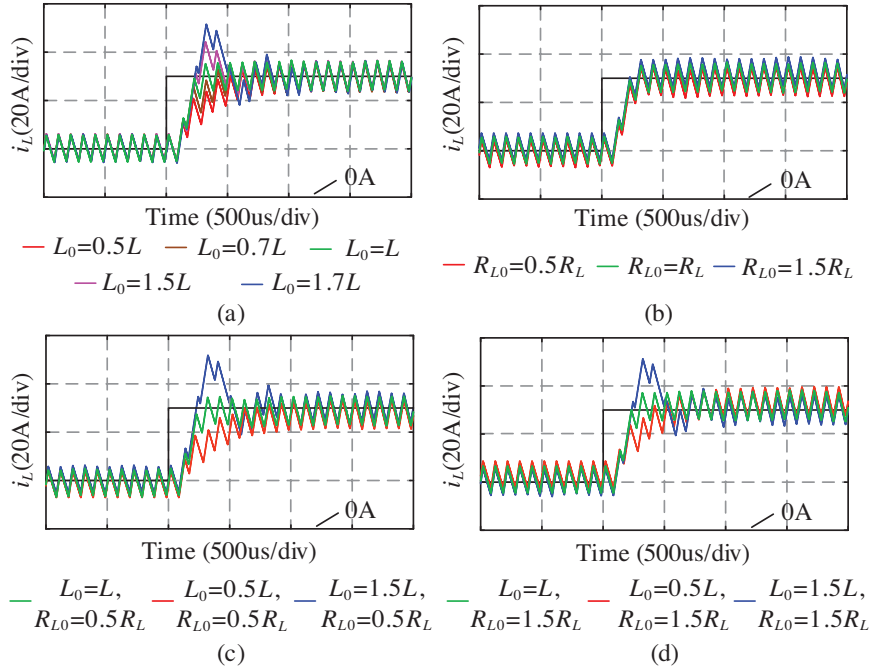


FIGURE 6 Step response of MPCC with parameter variation

If L_0 is less than L , the actual inductor current change will be less than the predicted change, which leads to a slower speed to track the current conference. If L_0 is larger than L , the actual inductor current change will be larger than the predicted change, which may lead to overshoot when the current reference changes abruptly.

Figure 6 shows the step response of MPCC with parameter variation. As shown in Figure 6a, there is no steady-state error when only the inductance is mismatched, but the dynamic tracking speed is affected. The larger the deviation $|\Delta L|$ of the inductance, the larger the impact on the dynamic tracking speed. The overshoot will occur when L_0 is larger than L . It can be seen from Figure 6b that the series resistance mismatch will generate the steady-state error. Compared with the results in Figure 6b, both the dynamic and steady-state performances of MPCC are affected in Figures 6c and 6d when the inductance and series resistance are both mismatched, the influence of these two cases on the steady-state error is different. If L_0 is less than L , $|\epsilon_{ss}|$ is larger than the corresponding result in Figure 6b when only the series resistance is mismatched. If L_0 is larger than L , $|\epsilon_{ss}|$ is smaller than the corresponding result in Figure 6b. Moreover, the influence of parameter mismatch on the steady-state error is consistent with the theoretical result shown in (12) and Figure 5.

In summary, the inductance mismatch mainly affects the dynamic control performance of MPCC that includes reduced tracking speed or large overshoot. The series resistance mismatch mainly causes the steady-state tracking errors. And the inductance mismatch will also affect tracking errors when the series resistance is mismatched. Therefore, the parameter mismatch should not be ignored.

4 | IMPROVED MPCC STRATEGY FOR THE FSBB CONVERTER CONSIDERING PARAMETER MISMATCH

In order to improve the robustness of MPCC to parameter mismatch and the dynamic performance of the multi-mode control for the FSBB converter, an improved MPCC strategy considering parameter mismatch is proposed, the control block diagram is shown in Figure 7. The outer loop is a voltage loop based on the PI controller, which stabilizes the output voltage V_o and calculates the inductor current reference $i_{L,\text{ref}}$. The inner loop is an improved MPCC strategy that can realize fast tracking of the inductor current reference and multi-mode switching control of the FSBB converter. The PDO is designed to correct prediction model in real time based on the estimated model deviations to reduce the influence of parameter mismatch. And the dynamic adjustment block related to the tracking error is used to further deal with dynamic performance degradation. In addition, the current feedforward based on the LDO is designed to improve the dynamic response of the converter to random load disturbances. It is worth noting that the observers are designed based on the prediction model, the prediction results of MPCC can be used in the calculation of the observers. Moreover, the implementation of the proposed strategy only requires the sampling results of $V_i(k)$, $V_o(k)$, $i_L(k)$. Therefore, the observers will not add much computational burden.

4.1 | Observers design considering parameter mismatch and random disturbances

The continuous-time model of inductor current for the FSBB converter considering the inductance and series resistance

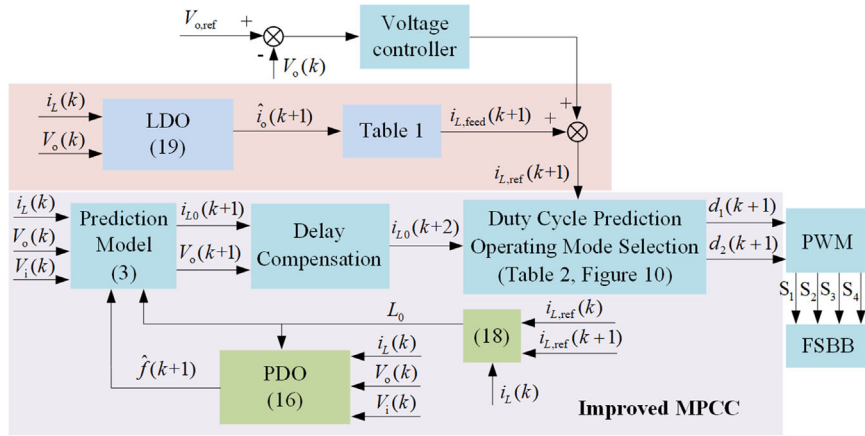


FIGURE 7 Improved MPCC strategy for multi-mode FSBB converter

mismatch can be expressed as

$$(L_0 + \Delta L) \frac{di_L(t)}{dt} = V_i(t)d_1(t) - V_o(t)[1 - d_2(t)] - i_L(t)(R_{L0} + \Delta R_L). \quad (14)$$

The deviations ΔL and ΔR_L are difficult to accurately measure when the converter is running. As a result, it is very difficult to establish an accurate prediction model. To this end, the model deviations caused by parameter mismatch are regarded as a kind of disturbance and used as a disturbance state variable in the prediction model. The disturbance state variable is defined as

$$f(t) = i_L(t)\Delta R_L + \Delta L \frac{di_L(t)}{dt}. \quad (15)$$

The PDO for the FSBB converter is designed based on the Luenberger observer to estimate the real-time parameter disturbance caused by parameter mismatch; the discrete-time model of the PDO is shown in (16). The error between the measured inductor current $i_L(k)$ and the observed inductor current $\hat{i}_L(k)$ is taken as the input variable of the PDO. By setting an appropriate gain matrix G , the error can be quickly driven to zero, so that the observed inductor current can quickly approach the real-time sampling result. Then, the estimated disturbance state $\hat{f}(k+1)$ is updated to the prediction model as the deviation between the prediction model and the actual FSBB converter system, so as to achieve the purpose of correcting the prediction model in real time. Through the above method, the open-loop MPCC becomes a closed-loop one with considering parameter mismatch, which makes the output of the prediction model closer to the actual circuit state and helps to eliminate the tracking errors due to parameter mismatch.

$$\begin{cases} \hat{x}(k+1) = A_d \hat{x}(k) + B_d \hat{v}(k) + G(y(k) - \hat{y}(k)) \\ \hat{y}(k) = C_d \hat{x}(k) \end{cases} \quad (16)$$

$$\begin{aligned} A_d &= \begin{bmatrix} 1 - \frac{R_{L0}T_s}{L_0} & -\frac{T_s}{L_0} \\ 0 & 1 \end{bmatrix}, \\ B_d &= \begin{bmatrix} \frac{T_s}{L_0}d_1(k) & -\frac{T_s}{L_0}[1 - d_2(k)] \\ 0 & 0 \end{bmatrix}, \\ C_d &= \begin{bmatrix} 1 & 0 \\ 0 & 1 \end{bmatrix}, \\ G &= \begin{bmatrix} g_1 & 0 \\ g_2 & 0 \end{bmatrix}. \end{aligned}$$

where $\hat{x}(k) = [\hat{i}_L(k) \ \hat{f}(k)]^T$, $\hat{v}(k) = [V_i(k) \ V_o(k)]^T$, $\hat{y}(k) = [\hat{i}_L(k) \ \hat{f}(k)]^T$, $y(k) = [i_L(k) \ f(k)]^T$, G is the observer gain matrix, A_d , B_d and C_d are the observer coefficient matrices.

Based on (6), the inductor current prediction model modified from the estimated result of the PDO can be expressed as

$$\begin{aligned} i_{L0}(k+1) &= \left(1 - \frac{R_{L0}T_s}{L_0}\right)i_L(k) - \frac{[1 - d_2(k)]T_s}{L_0}V_o(k) \\ &\quad + \frac{d_1(k)T_s}{L_0}V_i(k) - \frac{\hat{f}(k+1)T_s}{L_0} \end{aligned} \quad (17)$$

However, it is unavoidable that the observed result actually lags the sampling result during the dynamic process because the role of the observer is to make the observed result quickly approach the real-time sampling result. In addition, there is the control delay in the actual control process. The above factors limit the capability of the PDO to quickly estimate accurate model deviations when the current reference changes abruptly. But Figure 6 shows that the dynamic response process of MPCC is very short when the current reference changes. Hence, it is

not sufficient to rely only on the PDO to deal with the dynamic performance degradation due to parameter mismatch.

According to the analysis in Section 3, the main factor affecting the change of the dynamic performance of MPCC is the inductance L_0 of the prediction model. Therefore, adjusting L_0 properly during the dynamic process under the condition of ensuring the stability of MPCC can reduce the influence of parameter mismatch on the dynamic performance. For example, when the actual inductor current has not reached the reference during the dynamic process of tracking the current reference, L_0 can be increased according to the tracking error, which can speed up the tracking speed. The idea of this approach is to further adjust the prediction model to improve the dynamic performance of tracking the current reference with parameter mismatch during the dynamic process. The dynamic adjustment law is shown in (18). As shown in Figure 6, if the current reference changes when L_0 is larger than L , the overshoot will occur. If the possible overshoot cannot be suppressed or compensated in advance, it is difficult to avoid it due to the control delay and short dynamic process. In view of this, the overshoot can be avoided by first reducing L_0 at the moment of a significant sudden change in the current reference, which can make the actual inductor current change relatively less, then L_0 is adjusted according to the tracking error.

$$L_0 = \begin{cases} \delta_1 L_0 & |i_{L,\text{ref}}(k+1) - i_{L,\text{ref}}(k)| \geq \alpha \\ (\delta_2 + 1) L_0 & |i_{L,\text{ref}}(k+1) - i_{L,\text{ref}}(k)| < \alpha \end{cases} \quad (18)$$

$$\delta_2 = \begin{cases} 0 & 0 \leq i_{L,\text{RD}}(k) < \beta \\ i_{L,\text{RD}}(k) & \beta \leq i_{L,\text{RD}}(k) < 1 \\ 1/i_{L,\text{RD}}(k) & i_{L,\text{RD}}(k) \geq 1 \end{cases}$$

$$i_{L,\text{RD}}(k) = \left| \frac{i_{L,\text{ref}}(k+1) - i_L(k)}{i_L(k)} \right|.$$

where δ_1 and δ_2 are the adjustment coefficients. The constant α represents the degree of the current reference change. It makes the above adjustment process work when the current reference changes significantly; it will not affect the steady-state process. $i_{L,\text{RD}}(k)$ is the relative tracking error between the inductor current and its reference. The constant β is used to determine whether to adjust the coefficient δ_2 .

Through the cooperation of the PDO-based real-time correction and the dynamic adjustment block, the influence of parameter mismatch on the dynamic and steady-state control performances of MPCC can be reduced.

During the actual operation of the FSBB converter, the load variation is sometimes random and unpredictable. For this reason, the LDO is designed to observe the load variation in real time, as shown in (19). Then, the load observed result is converted into the inductor current $i_{L,\text{feed}}(k+1)$ corresponding to the current operating mode of the FSBB converter, as shown in Table 1. It is superimposed as a feedforward for the calcu-

TABLE 1 Inductor current feedforward

Operating mode	Inductor current feedforward value
Buck mode	$i_{L,\text{feed}}(k+1) = \hat{i}_o(k+1)$
E-Buck mode	$i_{L,\text{feed}}(k+1) = \hat{i}_o(k+1)/(1 - d_{2,\min})$
E-Boost mode	$i_{L,\text{feed}}(k+1) = \hat{i}_o(k+1)V_o(k)/V_i(k)/d_{1,\max}$
Boost mode	$i_{L,\text{feed}}(k+1) = \hat{i}_o(k+1)V_o(k)/V_i(k)$

lation of inductor current reference. This approach does not need to add the additional sensor, which can save the cost and improve the dynamic response of the FSBB converter when the load changes.

$$\begin{cases} \hat{\mathbf{x}}_o(k+1) = A_{\text{od}}\hat{\mathbf{x}}_o(k) + B_{\text{od}}\hat{\mathbf{v}}_o(k) + K_o(\mathbf{y}_o(k) - \hat{\mathbf{y}}_o(k)) \\ \hat{\mathbf{y}}_o(k) = C_{\text{od}}\hat{\mathbf{x}}_o(k) \end{cases} \quad (19)$$

$$A_{\text{od}} = \begin{bmatrix} 1 & -\frac{T_s}{C_2} \\ 0 & 1 \end{bmatrix}, \quad B_{\text{od}} = \begin{bmatrix} \frac{T_s[1 - d_2(k)]}{C_2} \\ 0 \end{bmatrix}, \quad C_{\text{od}} = \begin{bmatrix} 1 & 0 \\ 0 & 1 \end{bmatrix}, \quad K_o = \begin{bmatrix} k_1 & 0 \\ k_2 & 0 \end{bmatrix}.$$

where $\hat{\mathbf{x}}_o(k) = [\hat{V}_o(k) \ \hat{i}_o(k)]^T$, $\hat{\mathbf{v}}_o(k) = i_L(k)$, $\hat{\mathbf{y}}_o(k) = [\hat{V}_o(k) \ \hat{i}_o(k)]^T$, K_o is the observer gain matrix, A_{od} , B_{od} and C_{od} are the observer coefficient matrices.

The stability of the observer can be analyzed by deriving the characteristic matrix of the closed-loop system. The PDO and LDO are stable if all the characteristic roots of their characteristic matrix ($A_d - GC_d$) and ($A_{\text{od}} - K_o C_{\text{od}}$) are within the unit circle of the z-plane [15]. Additionally, the position of the characteristic roots will affect the performance of the observer.

The characteristic equation of the PDO can be written as

$$D(z) = |zI - (A_d - GC_d)|. \quad (20)$$

According to the Jury stability criterion, a feasible range of the gain coefficients g_1 and g_2 of the PDO can be derived as

$$\begin{cases} -\frac{R_{L0}T_s}{L_0} - \frac{g_2T_s}{L_0} < g_1 < 2 - \frac{R_{L0}T_s}{L_0} \\ -R_{L0} - \frac{g_1L_0}{T_s} < g_2 < 0 \end{cases}. \quad (21)$$

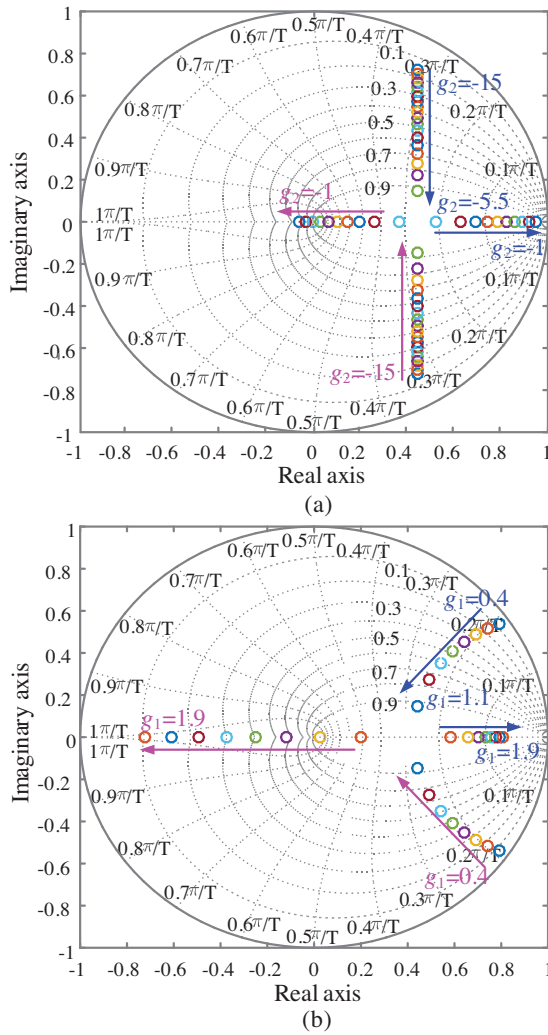


FIGURE 8 Characteristic roots of the PDO with different observer gains. (a) $g_1 = 1.1$ with varying g_2 . (b) $g_2 = -6$ with varying g_1 . PDO, parameter disturbance observer.

Similarly, the feasible range of the gain coefficients k_1 and k_2 of the LDO can be derived as

$$\begin{cases} -\frac{k_1 T_s}{C_2} < k_1 < 2 - \frac{k_1 T_s}{C_2} \\ -\frac{k_1 C_2}{T_s} < k_2 < 0 \end{cases}. \quad (22)$$

The distribution of the characteristic roots of the PDO and LDO in the z -plane with different observer gains can be depicted in Figures 8 and 9. When the characteristic roots are close to the origin, the response speed becomes faster; at the same time, it is more sensitive to the disturbance and noise. When the characteristic roots are close to the unit circle, the response speed slows down and the stability deteriorates. The appropriate gain coefficients of the observer will result in a good stability and performance. Hence, selecting the appropriate observer gains requires a comprehensive consideration on

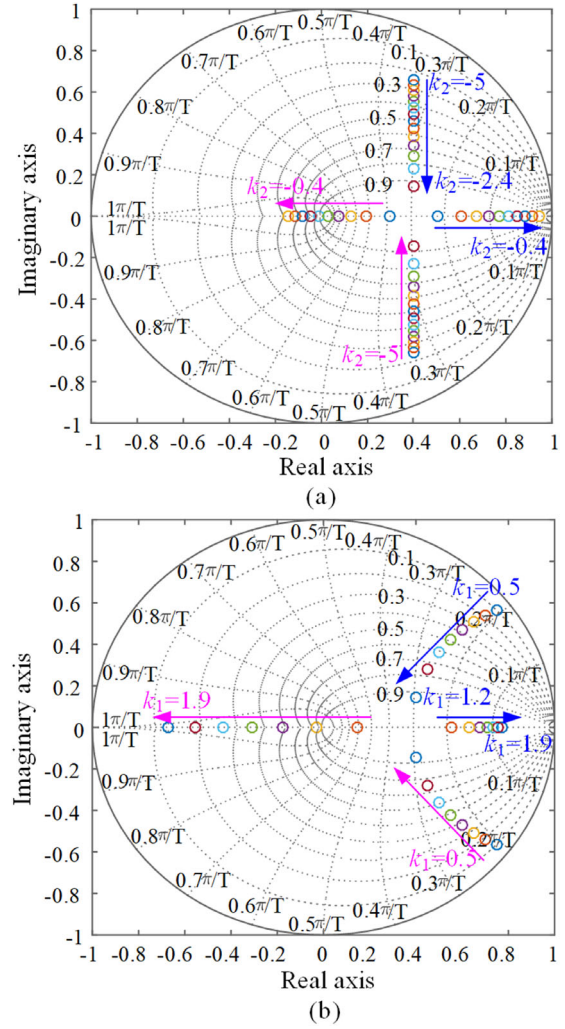


FIGURE 9 Characteristic roots of the LDO with different observer gains. (a) $k_1 = 1.2$ with varying k_2 . (b) $k_2 = -2.4$ with varying k_1 . LDO, load disturbance observer.

the disturbance sensitivity and response speed of the observer. The selection principle is usually to make the characteristic roots distributed in the right half of the unit circle and close to the origin. When the observer is stable, the error between the actual value and the observed result can be quickly driven to zero, so that the observer can accurately reflect the observed state change. Therefore, the prediction model of MPCC can be corrected in real time based on the estimated model deviations of the PDO and the control performance with parameter mismatch can be improved. As a result, the robustness of MPCC to parameter mismatch is improved.

4.2 | Multi-mode switching control based on MPCC

To achieve mode switching control of the FSBB converter without extra mode detection, the prediction mechanism of MPCC is used to automatically select the most suitable operating mode.

TABLE 2 Duty cycles of four operating modes

<i>M</i>	The duty cycle
Buck (<i>M</i> = 1)	$\begin{cases} d_1(k+1) = \frac{L_0[i_{L,\text{ref}} - i_{L,0}(k+2)] + [V_o(k+1) + i_{L,0}(k+2)R_{L,0} + \hat{f}(k+1)]T_s}{V_i(k+1)T_s} \\ d_2(k+1) = 0 \end{cases}$
E-Buck (<i>M</i> = 2)	$\begin{cases} d_1(k+1) = \frac{L_0[i_{L,\text{ref}} - i_{L,0}(k+2)] + [V_o(k+1)d_{2,\text{max}} + i_{L,0}(k+2)R_{L,0} + \hat{f}(k+1)]T_s}{V_i(k+1)T_s} \\ d_2(k+1) = d_{2,\text{min}} \end{cases}$
E-Boost (<i>M</i> = 3)	$\begin{cases} d_1(k+1) = d_{1,\text{max}} \\ d_2(k+1) = \frac{L_0[i_{L,\text{ref}} - i_{L,0}(k+2)] - [V_i(k+1)d_{1,\text{max}} - V_o(k+1) - i_{L,0}(k+2)R_{L,0} - \hat{f}(k+1)]T_s}{V_o(k+1)T_s} \end{cases}$
Boost (<i>M</i> = 4)	$\begin{cases} d_1(k+1) = 1 \\ d_2(k+1) = \frac{L_0[i_{L,\text{ref}} - i_{L,0}(k+2)] - [V_i(k+1) - V_o(k+1) - i_{L,0}(k+2)R_{L,0} - \hat{f}(k+1)]T_s}{V_o(k+1)T_s} \end{cases}$

Considering the control delay compensation, the predicted inductor current $i_{L,0}(k+2)$ of the four operating modes of the FSBB converter can be derived according to (3). Assuming that the inductor current can reach the reference $i_{L,\text{ref}}(k+1)$ in the next control period, the duty cycles $d_1(k+1)$ and $d_2(k+1)$ in the next control cycle if operating in the Buck, E-Buck, E-Boost or Boost mode can be obtained according to (5), respectively. The expressions of $d_1(k+1)$ and $d_2(k+1)$ are listed in Table 2, where $M = 1$ to 4, representing the Buck, E-Buck, E-Boost or Boost mode, respectively. In order to facilitate the selection process of the operating mode later, the duty cycles of the above four operating modes are noted as $d_{1,b}(k+1)$ and $d_{2,b}(k+1)$, $d_{1,eb}(k+1)$ and $d_{2,eb}(k+1)$, $d_{1,ebo}(k+1)$ and $d_{2,ebo}(k+1)$, $d_{1,bo}(k+1)$ and $d_{2,bo}(k+1)$, respectively.

According to the relationship between the duty cycles d_1 , d_2 and the operating modes of the FSBB converter shown in Figure 3, the most suitable operating mode can be selected in advance based on the duty cycle prediction results as shown in Figure 10. The duty cycle hysteresis is added near the mode boundary to avoid undesired mode switching. After determining the operating mode for the next control cycle, the number of the selected operating mode is recorded by the variable M . Then, the duty cycle commands $d_1(k+1)$ and $d_2(k+1)$ of the next control cycle are obtained by querying Table 2. Finally, they are updated to the switch actions in the next control cycle. It is noted that the proposed operating mode selection method is completed based on the prediction results of d_1 and d_2 ; there is no need for extra mode detection and separate control loops design for different operating modes.

Under the control of the above method, the voltage gain of the FSBB converter can be shown in Figure 11. A variable m is defined that can take values between 0 and 2 ($0 < m < 2$), the relationship between m and d_1 , d_2 is as follows: in the Buck mode, $d_{1,b} = m$; in the E-Buck mode, $d_{1,eb} = m - d_{2,bo}$; in the

E-Boost mode, $d_{2,ebo} = m - d_{1,max}$; and in the E-Boost mode, $d_{2,bo} = m - 1$. It can be seen that when the input and output voltages are close, the voltage gain is approximately continuous. In addition, the duty cycle hysteresis can avoid frequent mode switching near mode switching boundaries.

5 | SIMULATION VERIFICATION

The proposed strategy is tested in MATLAB/Simulation to verify its effectiveness on a 40-kW FSBB converter for a high-power application with the system parameters given in Table 3. According to the PI controller design method in [21], the PI parameters of this paper are designed. Both the normal conditions and parameter mismatch conditions are carried out.

5.1 | Step change in the current reference

Figure 12 shows the current tracking performance of the proposed strategy and the conventional PI control strategy. The input voltage is 900 V, the load is 15 Ω. It can be seen that the proposed strategy can adjust the inductor current to the new reference in about 0.4 ms without overshoot when the inductor current reference steps from 20 A to 40 A. Compared with PI control, the proposed MPCC has a faster current tracking speed. Figure 13 shows the current tracking performances with parameter mismatch under the control of the proposed strategy and the conventional MPCC strategy. As shown in Figures 13a and 13c, the inductance L_0 and series resistance $R_{L,0}$ mismatch results in steady-state tracking errors and reduced tracking speed when using the conventional MPCC strategy. Comparatively, there are no obvious tracking errors, a better dynamic tracking performance is realized with the proposed strategy.

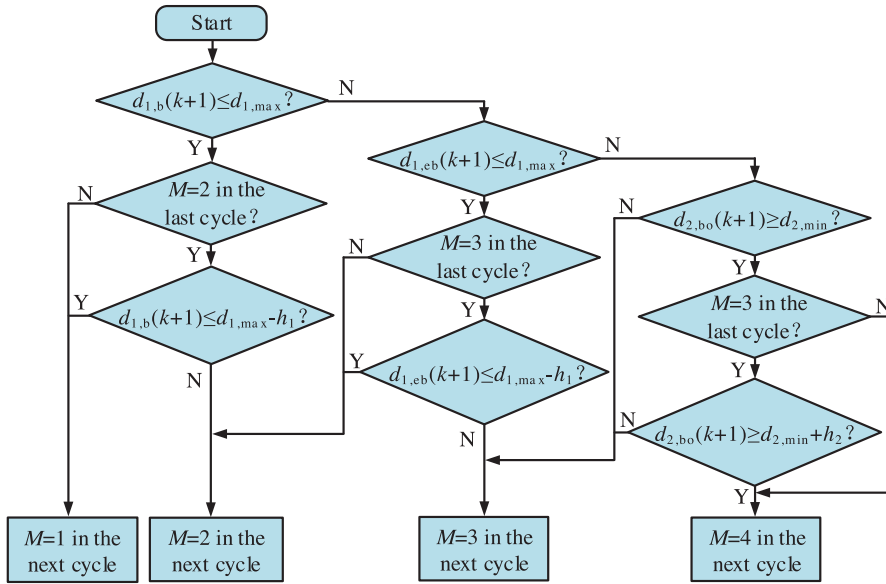


FIGURE 10 Flowchart of operating mode selection based on prediction results

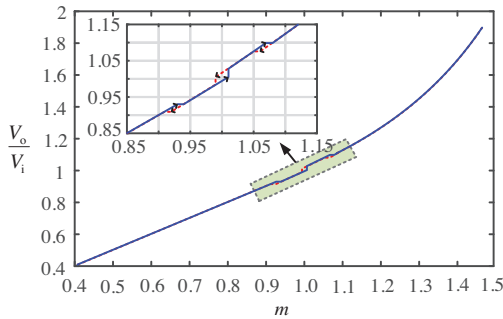


FIGURE 11 Voltage gain of the FSBB converter

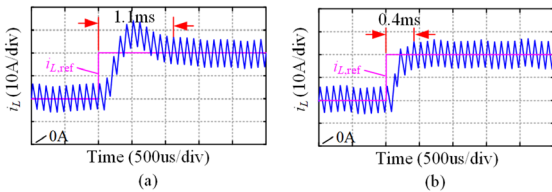


FIGURE 12 Simulation results of step change in the current reference. (a) PI control strategy. (b) Proposed strategy

TABLE 3 Simulation parameters

Parameter	Value	Parameter	Value
Input voltage, V_i /V	600–900	Output voltage reference, $V_{o,\text{ref}}$ /V	750
Inductor, L /mH	1.8	Maximum duty cycle, $d_{1,\text{max}}, d_{2,\text{max}}$	0.93
Input and output capacitances, C_1, C_2 /μF	630	Minimum duty cycle, $d_{1,\text{min}}, d_{2,\text{min}}$	0.07
Switching frequency, f_s /kHz	10	Duty cycle hysteresis width, b_1, b_2	0.03
Sampling period, T_s /μs	100	Adjustment coefficient, δ_1	0.5
Observer gain, G	$g_1 = 1.1$, $g_2 = -5$	Observer gain, K_o	$k_1 = 1.2$, $k_2 = -2.5$
Constant, α	10	Constant, β	0.2

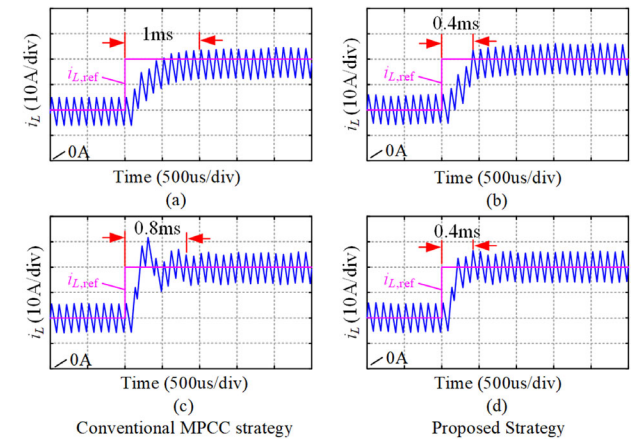


FIGURE 13 Simulation results of step change in the current reference with parameter mismatch. (a), (c) Conventional MPCC strategy. (b), (d) Proposed strategy. (a), (b) $L_0 = 0.5L$, $R_{L,0} = 0.5R_L$. (c) to (d) $L_0 = 1.5L$, $R_{L,0} = 0.5R_L$

The simulation results show that the proposed strategy can still achieve a better current tracking performance when the parameter mismatch exists.

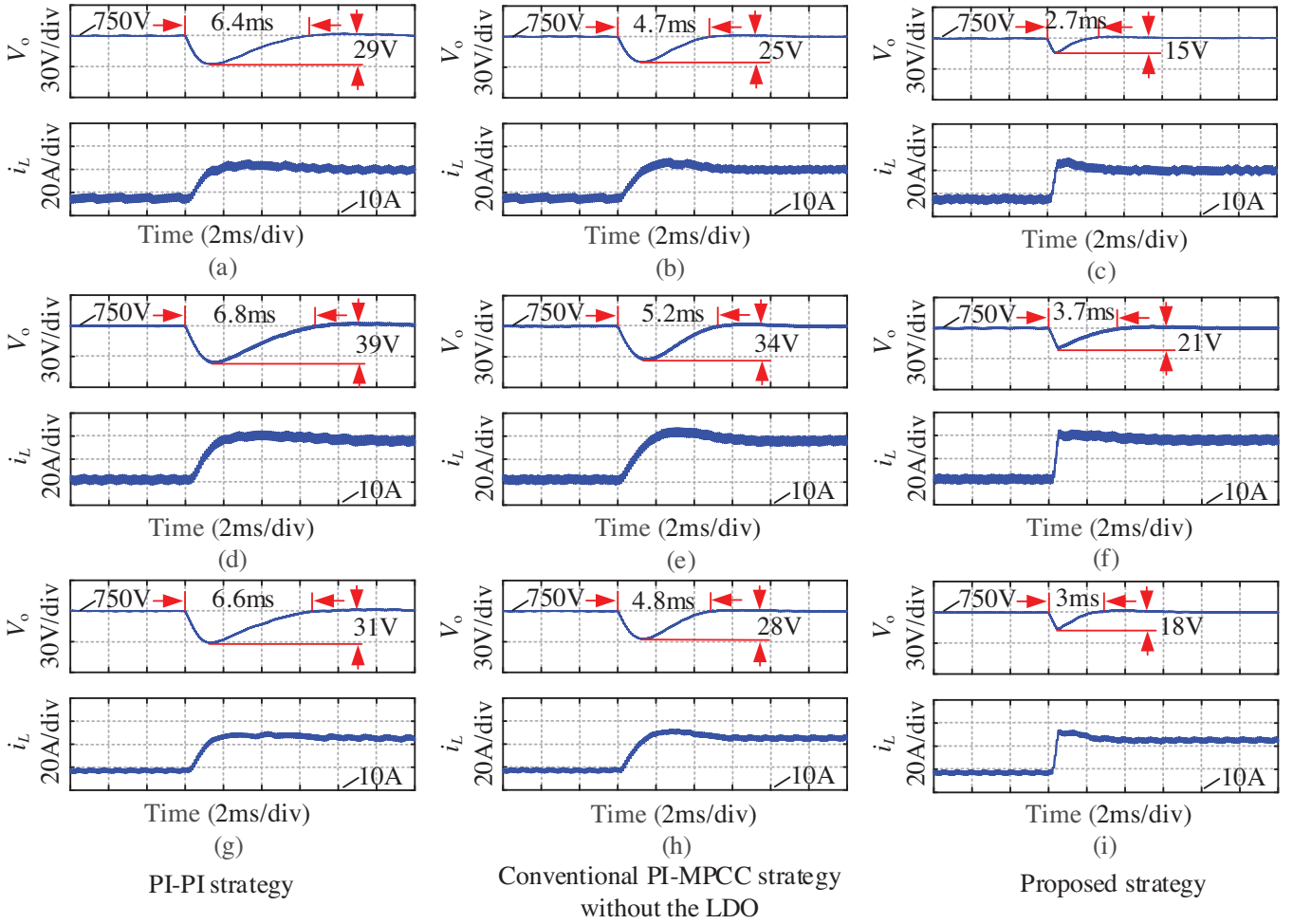


FIGURE 14 Simulation results of step change in load with different control strategies. (a,d,g) PI-PI strategy. (b,e,h) Conventional PI-MPCC strategy without the LDO. (c,f,i) Proposed strategy. (a to c) Buck mode with $V_i = 900$ V. (d to f) Boost mode with $V_i = 600$ V. (g to i) Extended mode with $V_i = 750$ V

5.2 | Step change in load

Figure 14 shows the simulation results when the load suddenly changes with the PI double-loop (PI-PI) strategy, conventional PI-MPCC strategy without the LDO and proposed strategy. The output voltage reference is 750 V. The initial load is 30Ω , then it steps to 15Ω . From the simulation results of the three operating modes, it can be seen that the dynamic control performances of both the MPCC-based strategies are better than those of the PI-PI strategy. Compared with the conventional PI-MPCC strategy without the LDO, the proposed strategy has a faster response speed and a smaller output voltage change during the dynamic process, which is because the proposed strategy adds the current feedforward based on the LDO. Therefore, the designed LDO can further improve the dynamic response of the proposed strategy to load disturbances.

Figure 15 shows the simulation results of step change in load in the Boost mode with parameter mismatch under the control of conventional PI-MPCC strategy with the LDO and proposed strategy. To better reflect the effectiveness of PDO

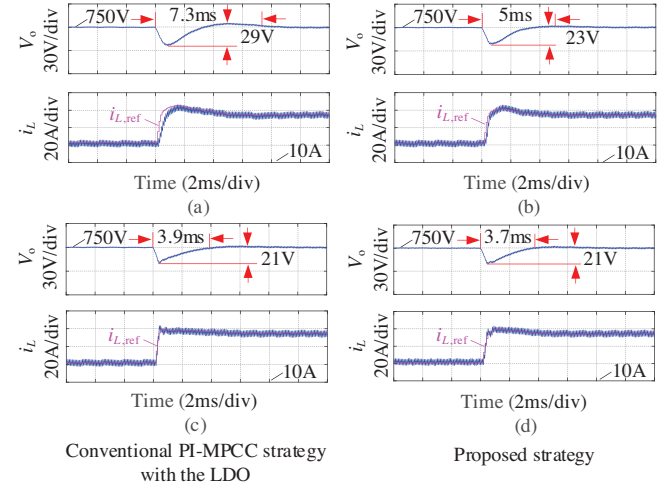


FIGURE 15 Simulation results of step change in load in the Boost mode with parameter variation. (a, c) Conventional PI-MPCC strategy with the LDO. (b, d) Proposed strategy. (a and b) $L_0 = 0.5 L$ and $R_{L,0} = 0.5 R_L$. (c and d) $L_0 = 1.5 L$ and $R_{L,0} = 0.5 R_L$

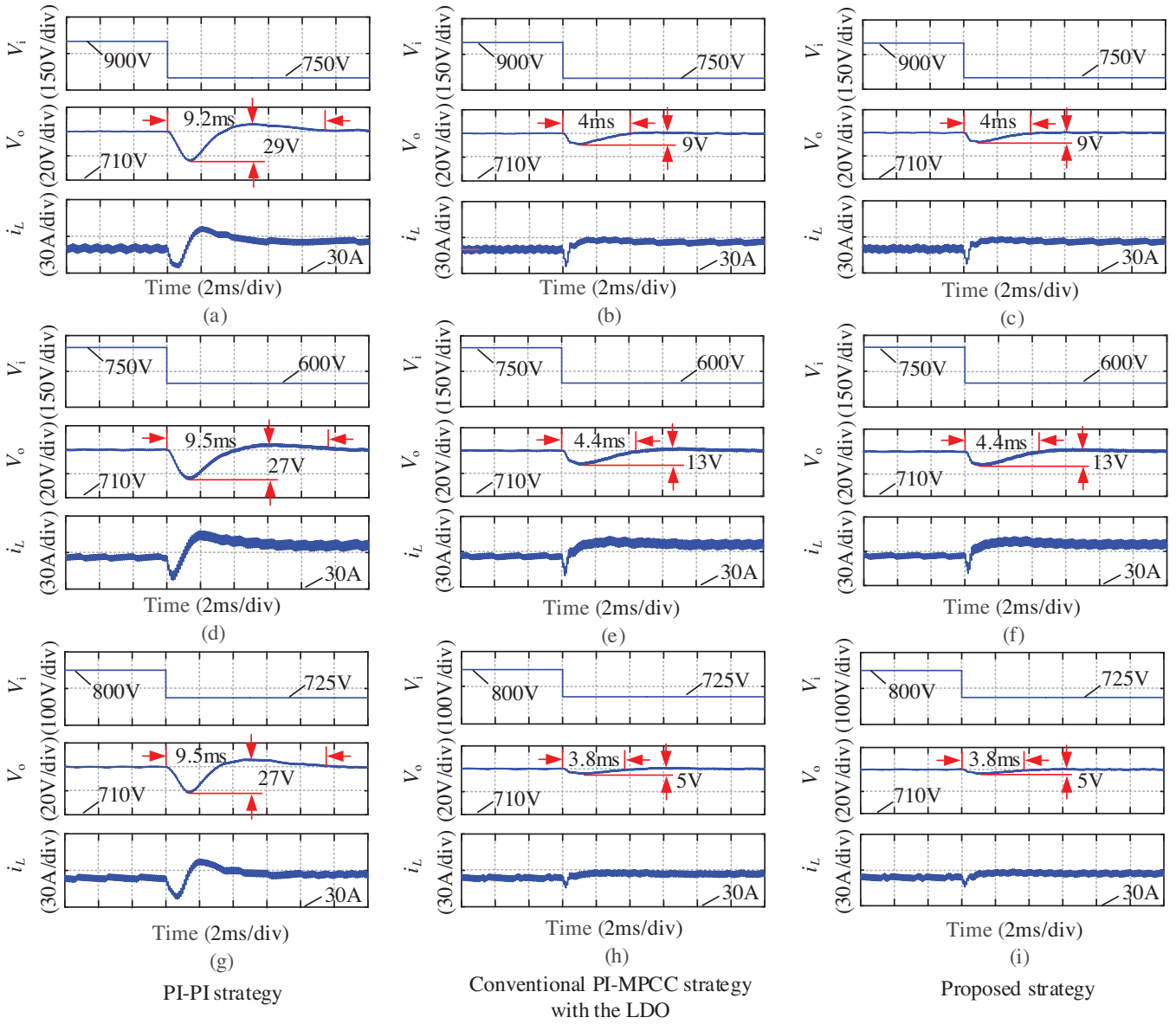


FIGURE 16 Simulation results of mode switching with different control strategies. (a, d, g) PI-PI strategy. (b, e, h) Conventional PI-MPCC strategy with the LDO; (c, f, i) Proposed strategy. (a to c) Buck mode switches to extended mode. (d to f) extended mode switches to Boost mode. (g to i) E-Buck mode switches to E-Boost mode

in the proposed strategy, the designed LDO is also added in the conventional PI-MPCC strategy. When the inductance L_0 and series resistance R_{L0} are both 50% of their actual values, the current tracking speed of the conventional MPCC strategy slows down and the tracking errors is obvious. As a result, the dynamic regulation process of the output voltage is affected. The dynamic output voltage variation is about 29 V in this condition. Comparatively, the proposed strategy can compensate for the effect of parameter mismatch based on the PDO. It can be found that the current tracking performance is better than the conventional MPCC strategy, the dynamic output voltage variation is about 23 V, which is reduced by about 20.7%. In addition, when L_0 is 150% of the actual value and R_{L0} is 50% of the actual value, it can be seen that such a parameter mismatch

has a slight effect on the current tracking performance of both the proposed strategy and the conventional PI-MPCC strategy, so the dynamic changes of output voltage are basically consistent. The simulation results show that the proposed strategy can achieve a relatively better dynamic performance with parameter mismatch when the load changes.

5.3 | Operating mode switching

Figure 16 shows the simulation results of operating mode switching among the Buck, Boost and extended modes with different control strategies. The output voltage reference is 750 V, the load is 15 Ω. It can be found from the simulation results that

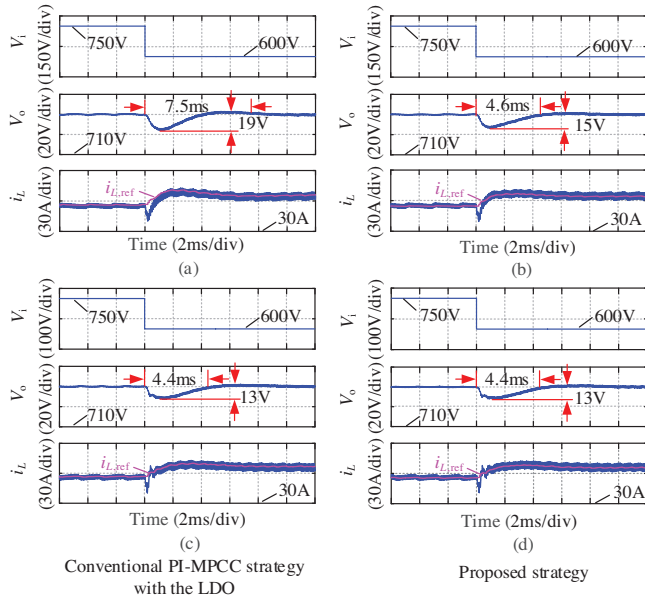


FIGURE 17 Simulation results of mode switching between the extended mode and Boost mode with parameter variation. (a and c) Conventional PI-MPCC strategy with the LDO. (b and d) Proposed strategy. (a and b) $L_0 = 0.5 L$ and $R_{L0} = 0.5 R_L$. (c and d) $L_0 = 1.5 L$ and $R_{L0} = 0.5 R_L$

the mode switching process is not smooth under the control of the PI-PI strategy. And the settling time to complete mode switching is obviously longer than the strategies with MPCC. It can also be seen that the conventional PI-MPCC strategy with the LDO has almost the same control effect as the proposed strategy. This is because there is no parameter mismatch in the above simulations. In addition, the proposed mode selection method shown in Figure 10 is also used in the conventional strategy. Hence, it can also verify the proposed strategy has a better mode switching performance.

The simulations of operating mode switching between the Boost and extended modes with parameter mismatch are carried out to further test the control performance of the proposed strategy when the model parameters are mismatched. From the simulation results shown in Figure 17, it can be seen that when L_0 is 150% of the actual value and R_{L0} is 50% of the actual value, the dynamic performances of both two strategies are basically consistent, because such a parameter mismatch has a slight effect on the current tracking performance of both two strategies. But the dynamic performances of mode switching under the conventional PI-MPCC strategy are obviously affected when the inductance L_0 and the series resistance R_{L0} are both 50% of their actual values compared with the results shown in Figure 16. The dynamic output voltage change is about 19 V, the settling time becomes longer. It can be seen that the dynamic output voltage variation is about 15 V with the proposed strategy, which is reduced by 21.1%, the settling time is about 4.6 ms. Therefore, the simulation results demonstrate that the proposed strategy can still realize a relatively better mode switching performance with parameter mismatch.

6 | EXPERIMENTAL VERIFICATION

The effectiveness of the proposed strategy is further evaluated by experiments with the system parameters listed in Table 4. The experimental platform is shown in Figure 18, which consists of a FSBB converter, a DC supply, an oscilloscope, the resistive loads. All the control strategies are implemented by the dSPACE DS1103 and a slave digital signal processor pulse width modulation (PWM) generation of the dSPACE to generate the PWM signals in the experiments. The maximum and minimum values of d_1 and d_2 are the same as Table 3.

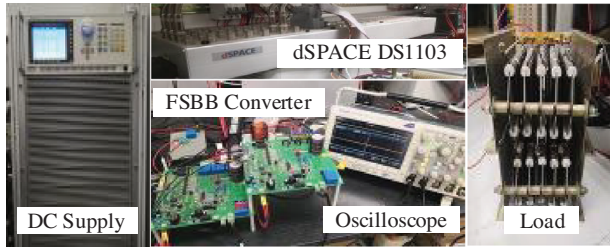
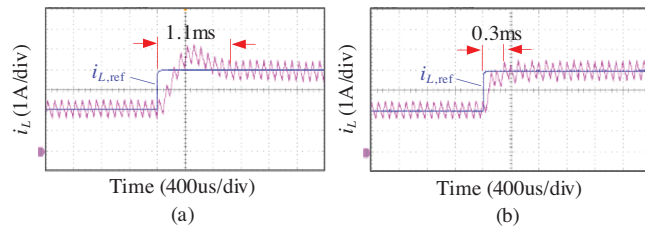
6.1 | Step change in the current reference

Figure 19 shows the experimental results of step change in the inductor current reference with the proposed strategy and conventional PI control strategy. The input voltage is 130 V, the load is 20Ω . It can be seen that the proposed strategy can adjust the inductor current to the new reference in about 0.3 ms without overshoot when the inductor current reference steps from 2 to 4 A. Comparatively, it takes about 1.1 ms for the inductor current to track to the reference and a significant overshoot can be observed under the PI control strategy. The proposed strategy has a faster current control performance than the PI control due to the predictive capability.

Figure 20 shows the experimental results of step change in the current reference with parameter mismatch when using the proposed strategy and the conventional MPCC strategy. Table 5 lists the control performances of the two strategies. It can be seen that the parameter mismatch will cause steady-state errors in the conventional MPCC strategy and affect its dynamic control performance, which is consistent with theoretical analysis and simulations. For example, the inductance L_0 and series resistance R_{L0} are both less than their actual values in Figures 20a and 20c, which leads to tracking errors and slower dynamic response in the conventional MPCC strategy. As shown in Figures 20e and 20g, L_0 is larger than its actual value and R_{L0} is less than its actual value, which results in tracking errors and overshoot. Based on the conventional MPCC strategy, the proposed strategy adds the PDO and dynamic adjustment block to improve the control performance of tracking the current reference change when the parameter mismatch exists. It can be seen from Figures 20b and 20f, the tracking errors are eliminated under the proposed strategy because the prediction model of the MPCC can be corrected based on the observed model deviations of the PDO. According to the analysis in Section 3, the main factor affecting the steady-state errors is the resistance mismatch. According to the definition of the observed parameter disturbance state shown in (15), the theoretical \hat{f} is about 1 V when the inductor current is 4 A, R_{L0} has a 50% error (0.25Ω) and the influence of inductance mismatch on steady-state error is ignored, which is basically consistent with the experimental results shown in Figures 20b and 20f. As shown in Figures 20d and 20h, the dynamic tracking performance is also improved with the quick dynamic adjustment

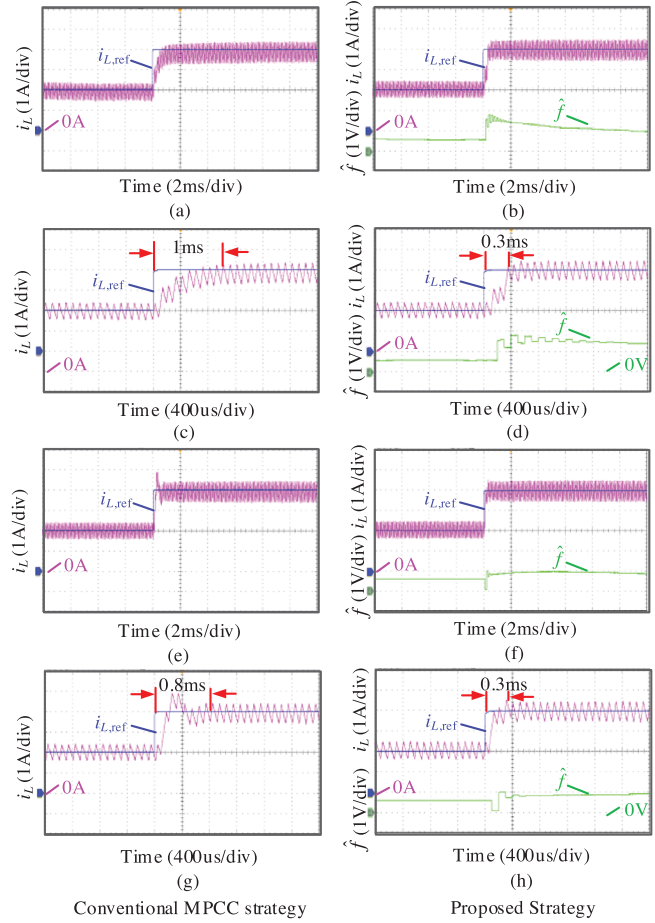
TABLE 4 Experimental parameters

Parameter	Value	Parameter	Value
Input voltage, V_i /V	90–130	Output voltage reference, $V_{o,\text{ref}}$ /V	110
Inductor, L /mH	3.3	Series resistance, R_L /Ω	0.5
Input and output capacitances, C_1, C_2 /μF	470	Adjustment coefficient, δ_1	0.5
Switching frequency, f_s /kHz	10	Observer gain, G	$g_1 = 1.1$, $g_2 = -10$
Sampling time, T_s /μs	100	Observer gain, K_o	$k_1 = 1.2$, $k_2 = -1.8$
Constant, α	0.5	Constant, β	0.2

**FIGURE 18** Experimental platform**FIGURE 19** Experimental results of step change in the current reference. (a) PI control strategy. (b) Proposed strategy**TABLE 5** Performance comparison of tracking the current reference with parameter mismatch

Parameter mismatch	Performance	Conventional MPCC strategy	Proposed strategy
$L_0 = 0.5L$, $R_{L0} = 0.5R_L$	Settling time/ms	1.0	0.3
	Overshoot/A	≈ 0	≈ 0
	Deviation/A	0.15	≈ 0
$L_0 = 1.5L$, $R_{L0} = 0.5R_L$	Settling time/ms	0.8	0.3
	Overshoot/A	1.0	≈ 0
	Deviation/A	0.05	≈ 0

of the proposed strategy when the parameter mismatch exists. From the duty cycle expressions in Table 2, it can be found that the dynamic adjustment is to quickly adjust the duty cycle to compensate for the effects of parameter mismatch, especially the influence of inductance mismatch. For example, when the inductance L_0 is less than its actual value, the duty cycle

**FIGURE 20** Experimental results of step change in the current reference with parameter mismatch. (a), (c), (e) and (g) Conventional MPCC strategy. (b), (d), (f) and (h) Proposed strategy. (a) to (d) $L_0 = 0.5L$, $R_{L0} = 0.5R_L$. (e) to (h) $L_0 = 1.5L$, $R_{L0} = 0.5R_L$

obtained from the mismatched prediction model is less than that with no parameter mismatch occurring. Under the proposed strategy, it can be seen from Figures 20d and 20h that the observed \hat{f} can respond quickly to compensate for such mismatch so that the current tracking response is less affected. The experimental results show that the proposed strategy can reduce the influence of the inductance and resistance mismatch and realize a better control performances of the tracking current reference.

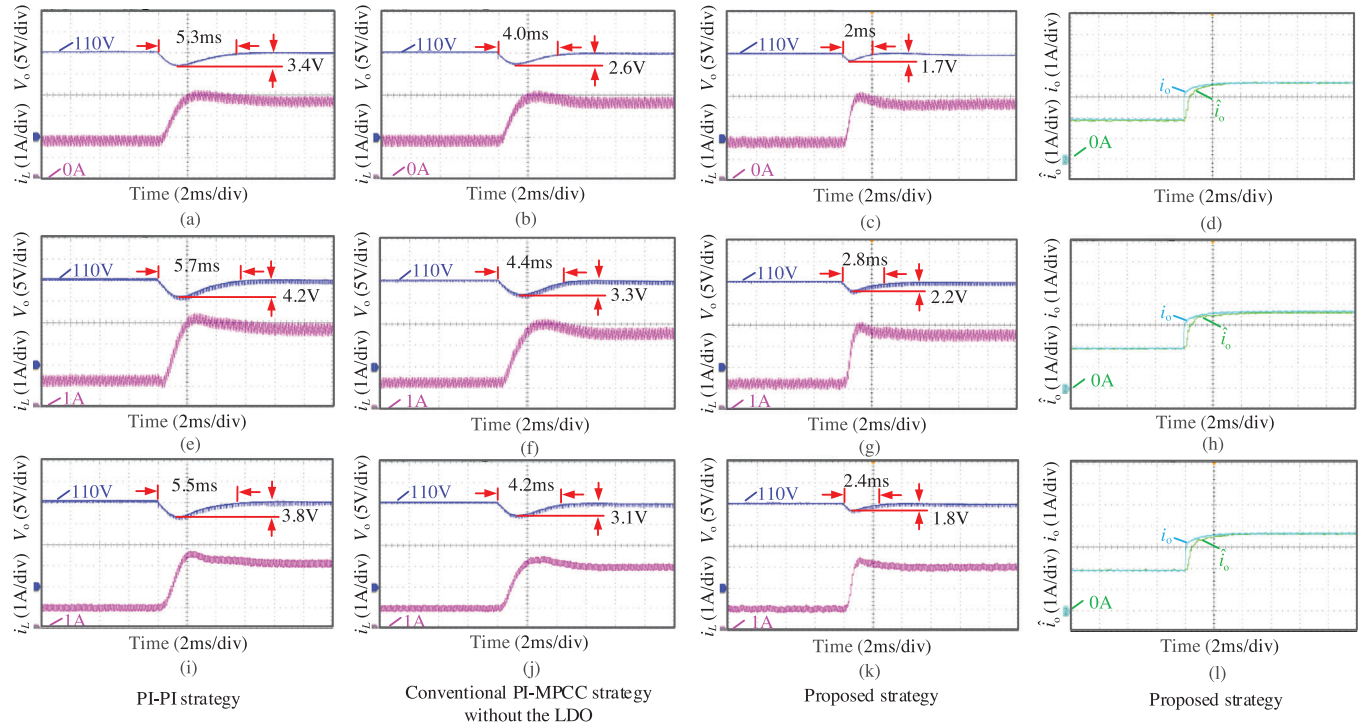


FIGURE 21 Experimental results of step change in load with different control strategies. (a, e, i) PI-PI strategy. (b, f, j) Conventional PI-MPCC strategy without the LDO. (c, g, k) Proposed strategy. (a to d) Buck mode with $V_i = 130$ V. (e to h) Boost mode with $V_i = 90$ V. (i to l) Extended mode with $V_i = 110$ V. (d, h, l) Measured load current and observed load current of the LDO in the proposed strategy

TABLE 6 Performance comparison of load step change

Operating mode	Performance	PI-PI	Conventional PI-MPCC without the LDO	Proposed strategy
Buck mode	Change in V_o/V	3.4	2.6	1.7
	Settling time/ms	5.3	4.0	2.0
Boost mode	Change in V_o/V	4.2	3.3	2.2
	Settling time/ms	5.7	4.4	2.8
Extended mode	Change in V_o/V	3.8	3.1	1.8
	Settling time/ms	5.5	4.2	2.4

6.2 | Step change in load

Figure 21 shows the experimental results of step change in load with the PI double-loop (PI-PI) strategy, conventional PI-MPCC strategy without the LDO and proposed strategy. Table 6 summarizes the control performances of different control strategies. The output voltage reference is 110 V. The initial load is 60Ω , then it steps to 30Ω . Figures 21a to 21d are the experimental results when the FSBB converter operates in the Buck mode, the input voltage is 130 V. It can be observed that the proposed strategy adjusts the output voltage back to the reference in about 2 ms, the output voltage changes about 1.7 V during the dynamic process. With the conventional PI-MPCC strategy without the LDO, it takes about 4.0 ms for the output voltage to return to the reference with a 2.6-V change. While using the PI-PI strategy, the settling

time is about 5.3 ms, the output voltage changes about 3.4 V. From the experimental results of the three operating modes, it can be known that the dynamic control performances of the MPCC-based strategies are better than those of the PI-PI strategy when the load changes abruptly. In addition, the proposed strategy adds the current feedforward based on the LDO. From the experimental results shown in Figures 21d, 21h and 21l, it can be found that the observed load current \hat{i}_o of the LDO in the proposed strategy can quickly track the actual load current i_o in the different operating modes. Hence, the designed LDO can effectively estimate the change of load current. The experimental results show that the response speed is faster when the load changes under the control of the proposed strategy, the output voltage is less affected compared with the conventional PI-MPCC strategy without the LDO.

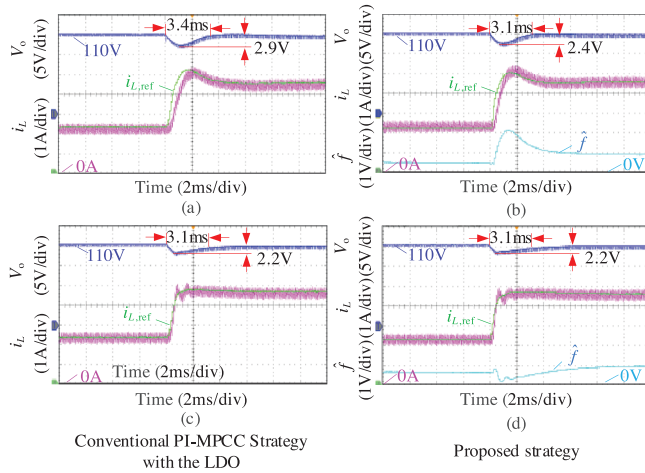


FIGURE 22 Experimental results of step change in load in the Boost mode with parameter variation. (a, c) Conventional PI-MPCC strategy with the LDO. (b, d) Proposed strategy. (a and b) $L_0 = 0.5 L$ and $R_{L0} = 0.5 R_L$. (c and d) $L_0 = 1.5 L$ and $R_{L0} = 0.5 R_L$

In order to verify the effectiveness of the proposed strategy in the case of parameter mismatch, the experiments of step change in load with parameter variation are carried out. For the fairness of comparison, the LDO is also added to the conventional PI-MPCC strategy in the experiments. Figure 22 shows the experimental results of the proposed strategy and the conventional PI-MPCC strategy with the LDO in the Boost mode. The experimental results in other modes are similar to them. In Figures 22a and 22b, the inductance L_0 and series resistance R_{L0} are both 50% of their actual values. Compared with the experimental results shown in Figure 21g, the dynamic control performances are degraded. Due to the voltage controller of the outer loop, even if there is a parameter mismatch in the prediction model, the output voltage can eventually stabilize at the reference under the above two strategies. According to the analysis in Section 3, the above parameter mismatch reduces the speed of MPCC to track the current reference and generates tracking errors, which will affect the dynamic regulation process of the outer loop. It can be observed from Figure 22a that the tracking speed of the current reference is slower, the tracking error of the inductor current appears under the control of the conventional PI-MPCC strategy with the LDO. But the proposed strategy is less affected because it can quickly compensate for the effect of parameter mismatch based on the observed results of the PDO. The above results are also consistent with theoretical analysis and simulations. During the dynamic process, the output voltage change is about 2.9 V with the conventional PI-MPCC strategy with the LDO; it is about 2.4 V using the proposed strategy. In Figures 22c and 22d, L_0 is 150% of the actual value and R_{L0} is 50% of the actual value. It can be observed that such a parameter mismatch has a slight effect on the control performance of the proposed strategy and the conventional PI-MPCC strategy when a step change in the load occurs. This is because the current tracking errors caused by the above parameter mismatch are small, which leads to less influence on the control performance of the

outer loop. From the experimental results, it also can be found that the observed disturbance state \hat{f} can quickly respond to improve the tracking capability of MPCC. Hence, the experimental results demonstrate that the proposed strategy still has a better control performance when the load changes abruptly under the condition of parameter mismatch.

6.3 | Operating mode switching

The experimental results of operating mode switching with different control strategies are shown in Figure 23. The control performances are summarized in Table 7. The output voltage reference is 110 V, the load is 30Ω . When the input voltage changes over a wide range, the FSBB converter will switch operating modes among the Buck, Boost and extended modes. For example, as shown in Figures 23a to 23c, when the input voltage steps from 130 to 110 V, the FSBB converter switches from the Buck mode to extended mode. It can be seen that the settling time to complete such a mode switching is about 3.2 ms, there is a 0.9-V change in the output voltage with the proposed strategy. The dynamic process of mode switching when using the conventional PI-MPCC strategy with the LDO is basically the same as the proposed strategy. This is because the above experiments are carried out without parameter mismatch; the mode selection method shown in Figure 10 is also used in the conventional strategy. While the PI-PI strategy is used, it takes about 8.5 ms to complete the mode switching and the output voltage changes about 5.6 V, which are longer and more than the proposed strategy. The experimental results show that the proposed strategy can complete mode switching more quickly. Moreover, it can realize smoother mode switching with smaller variations in the output voltage and inductor current during the dynamic switching process.

To further validate the effectiveness of the proposed strategy with parameter mismatch, this part conducts the mode switching experiments between the extended mode and the Boost mode as an example to illustrate the control effect of the strategies with parameter mismatch. The experimental results of the proposed strategy and the conventional PI-MPCC strategy with the LDO are shown in Figure 24. The experimental results of other mode switching are similar to them. In Figures 24a and 24b, the inductance L_0 and series resistance R_{L0} are both 50% of their actual values. When adopting the conventional PI-MPCC strategy with the LDO, the tracking speed of MPCC becomes slower due to parameter mismatch, which leads to an increase in the settling time of mode switching compared to the corresponding experimental results shown in Figure 23. The smoothness of mode switching is also affected. As shown in Figure 24a, this is because the parameter mismatch reduces the tracking performance of conventional MPCC to track the current reference and generates tracking errors, which will also affect the dynamic response of the voltage control. As a result, the dynamic output voltage change is about 2.3 V. But it can be observed that the proposed strategy is less affected by parameter mismatch than the conventional MPCC strategy, the dynamic output voltage change is about 1.9 V. In Figures 24c

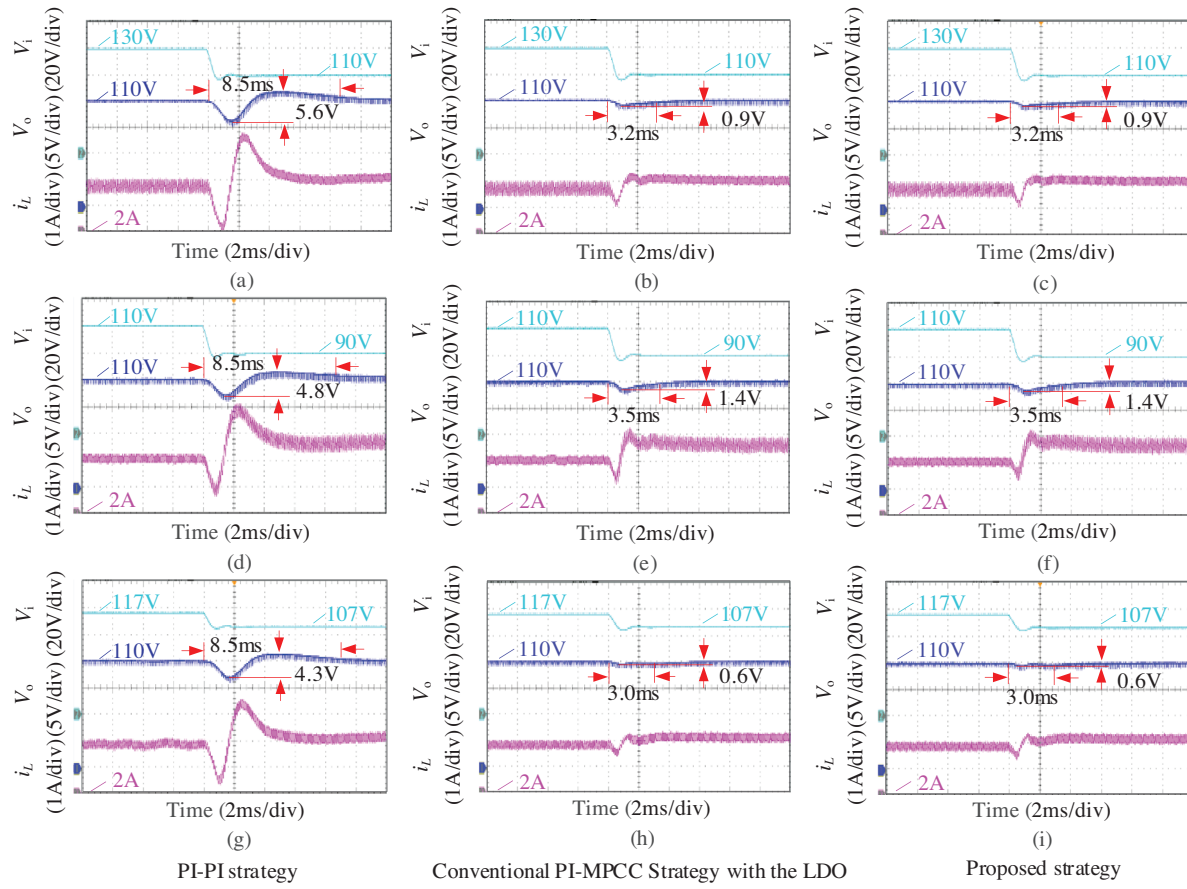


FIGURE 23 Experimental results of mode switching with different control strategies. (a, d, g) PI-PI strategy. (b, e, h) Conventional PI-MPCC strategy with the LDO; (c, f, i) proposed strategy. (a to c) Buck mode switches to extended mode. (d to f) Extended mode switches to Boost mode. (g to i) E-Buck mode switches to E-Boost mode

TABLE 7 Performance comparison of operating mode switching

Operating mode	Performance	PI-PI	Conventional PI-MPCC with the LDO	Proposed strategy
Buck → Extended	Change in V_o/V	5.6	0.9	0.9
	Settling time/ms	8.5	3.2	3.2
Extended → Boost	Change in V_o/V	4.8	1.4	1.4
	Settling time/ms	8.5	3.5	3.5
E-Buck → E-Boost	Change in V_o/V	4.3	0.6	0.6
	Settling time/ms	8.5	3.0	3.0

and 24d, L_0 is 150% of the actual value and R_{L0} is 50% of the actual value. It can be seen that such a parameter mismatch is not obvious in this condition so that the control performances of the above two strategies during mode switching are basically not affected. The experimental results demonstrate that the proposed strategy still has a good control performance for mode switching under the condition of parameter mismatch.

To sum up, the experimental conclusions are basically the same as simulations, which further verify the proposed strategy

can realize multi-mode operation of the FSBB converter with high control performances.

7 | CONCLUSION

In this paper, an improved MPCC strategy for the FSBB converter considering parameter mismatch is presented. The main conclusions are summarized as follows:

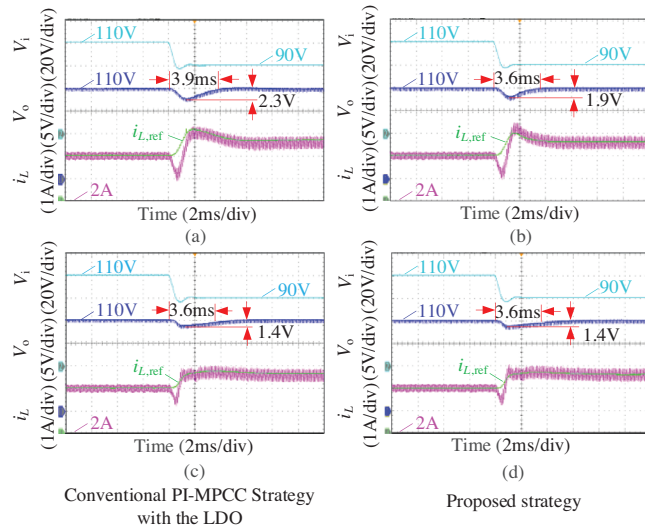


FIGURE 24 Experimental results of mode switching between the extended mode and Boost mode with parameter variation. (a and c) Conventional PI-MPCC strategy with the LDO. (b and d) Proposed strategy. (a and b) $L_0 = 0.5 L$ and $R_{L0} = 0.5 R_L$. (c and d) $L_0 = 1.5 L$ and $R_{L0} = 0.5 R_L$

1. The theoretical tracking error of MPCC due to parameter mismatch is derived; the influence of parameter mismatch on the dynamic performance is analyzed in detail. The results indicate that the inductance mismatch will affect the dynamic performance including reduced tracking speed or large overshoot; the inductance and series resistance mismatch may lead to tracking errors.
2. An improved MPCC strategy combined with the PDO and dynamic adjustment block is proposed. Based on the estimated model deviation of the PDO, the prediction model can be corrected so that the tracking errors caused by parameter mismatch can be eliminated. The dynamic adjustment block related to the tracking error can further avoid dynamic performance degradation. As a result, the proposed strategy can still retain good control performances with parameter mismatch compared with the conventional MPCC strategy. Additionally, the current feedforward based on the LDO can effectively improve the dynamic response of the converter to random load disturbances.
3. The multi-mode switching control of the FSBB converter is realized with the proposed MPCC, which can select the operating mode according to the prediction results of the duty cycles in the next control cycle without extra mode detection. Compared with the multi-mode control strategy using PI control, it can achieve smoother mode switching with high dynamic performance.

The simulation and experimental results demonstrate that the proposed strategy can improve the dynamic and steady-state performances of MPCC with parameter mismatch and achieve multi-mode operation of the FSBB converter with high control performances. The proposed strategy facilitates the applications of FSBB converters in high-power energy storage systems and other fields.

AUTHOR CONTRIBUTIONS

Yan Wu: Investigation; Methodology; Software; Validation; Writing—original draft. Wei Wang: Conceptualization; Supervision; Writing—review & editing. Fen Tang: Data curation; Project administration; Writing—review & editing. Xuezhi Wu: Project administration; Writing—review & editing. Zhe Chen: Conceptualization; Writing—review & editing. Long Jing: Funding acquisition; Resources. Weige Zhang: Funding acquisition; Resources.

ACKNOWLEDGEMENT

This work was supported by Delta Power Electronics Science and Education Development Plan (DREK2021005).

CONFLICT OF INTEREST

No conflicts of interest.

DATA AVAILABILITY STATEMENT

Research data are not shared.

REFERENCES

1. Wei, C.-L., Chen, C.-H., Wu, K.-C., Ko, I.-T.: Design of an average-current-mode noninverting buck-boost DC-DC converter with reduced switching and conduction losses. *IEEE Trans. Power Electron.* 27(12), 4934–4943 (2012)
2. Jones, D.C., Erickson, R.W.: Buck-Boost converter efficiency maximization via a nonlinear digital control mapping for adaptive effective switching frequency. *IEEE J. Emerg. Sel. Topics Power Electron.* 1(3), 153–165 (2013)
3. Aharon, I., Kuperman, A., Shmilovitz, D.: Analysis of dual-carrier modulator for bidirectional noninverting buck-boost converter. *IEEE Trans. Power Electron.* 30(2), 840–848 (2015)
4. Wu, K.-C., Wu, H.-H., Wei, C.-L.: Analysis and design of mixed-mode operation for non-inverting buck-boost DC-DC converters. *IEEE Trans. Circuits Syst. II Exp. Briefs* 62(12), 1194–1198 (2015)
5. Jia, L., Sun, X., Zheng, Z., Ma, X., Dai, L.: Multimode smooth switching strategy for eliminating the operational dead zone in noninverting buck-boost converter. *IEEE Trans. Power Electron.* 35(3), 3106–3113 (2020)
6. Liu, F., Zhao, Y., Wu, Z., Wang, W., Wang, H., Li, H.: Interleaved bidirectional Buck-Boost DC-DC converter based on multi-mode control. In: *Proceedings of International Conference on Green Energy and Applications*, pp. 182–186 (2022)
7. Wang, D., Wang, Z., Peng, Z., Zhang, Y., Cheng, X.-F.: A four-phase interleaved Buck-Boost converter with changed load connection for the fuel cell activation. *IEEE Access* 9, 102104–102113 (2021)
8. Restrepo, C., Calvente, J., Cid-Pastor, A., Aroudi, A.E., Giral, R.: A noninverting buck-boost DC-DC switching converter with high efficiency and wide bandwidth. *IEEE Trans. Power Electron.* 26(9) (2011)
9. Zhang, G., Yuan, J., Yu, S.S., Zhang, N., Wang, Y., Zhang, Y.: Advanced four-mode-modulation-based four-switch non-inverting buck-boost converter with extra operation zone. *IET Power Electron.* 13(10), 2049–2059 (2020)
10. Tsai, Y.-Y., Tsai, Y.-S., Tsai, C.-W., Tsai, C.-H.: Digital noninverting-buck-boost converter with enhanced duty-cycle-overlap control. *IEEE Trans. Circuits Syst. II Exp. Briefs* 64(1), 41–45 (2017)
11. Wang, Y., Lan, J., Huang, X., Fang, T., Ruan, X., Dong, M.: An improved single-mode control strategy based on four-switch buck-boost converter. In: *Proceedings of IEEE Applied on Power Electronics Conference and Exposition*, pp. 320–325 (2020)
12. Ren, X., Ruan, X., Qian, H., Li, M., Chen, Q.: Three-mode dual-frequency two-edge modulation scheme for four-switch buck-boost converter. *IEEE Trans. Power Electron.* 24(2), 499–509 (2009)
13. Tsai, C.-H., Tsai, Y.-S., Liu, H.-C.: A stable mode-transition technique for a digitally controlled non-inverting buck-boost DC-DC converter. *IEEE Trans. Ind. Electron.* 62(1), 475–483 (2015)

14. Restrepo, C., Konjedic, T., Calvente, J., Giral, R.: Hysteretic transition method for avoiding the dead-zone effect and subharmonics in a non-inverting buck-boost converter. *IEEE Trans. Power Electron.* 30(6), 3418–3430 (2015)
15. Cheng, L., et al.: Model predictive control for DC-DC boost converters with reduced-prediction horizon and constant switching frequency. *IEEE Trans. Power Electron.* 33(10), 9064–9075 (2018)
16. Kouro, S., Perez, M.A., Rodriguez, J., Llor, A.M., Young, H.A.: Model predictive control: MPC's role in the evolution of power electronics. *IEEE Ind. Electron. Mag.* 9(4), 8–21 (2015)
17. Huangfu, Y., Guo, L., Ma, R., Gao, F.: An advanced robust noise suppression control of bidirectional DC-DC converter for fuel cell electric vehicle. *IEEE Trans. Transp. Electrific.* 5(4), 1268–1278 (2019)
18. Zhou, D., Yang, S., Tang, Y.: Model-predictive current control of modular multilevel converters with phase-shifted pulselwidth modulation. *IEEE Trans. Ind. Electron.* 66(6), 4368–4378 (2019)
19. Karamanakos, P., Liegmann, E., Geyer, T., Kennel, R.: Model predictive control of power electronic systems: Methods, results, challenges. *IEEE Open J. Ind. Appl.* 1, 94–114 (2020)
20. Leng, Z., Liu, Q.: A simple model predictive control for buck converter operating in CCM. In: Proceedings of IEEE International Symp. Predictive Control Elect. Drives Power Electronics, pp. 19–24 (2017)
21. Restrepo, C., Garcia, G., Flores-Bahamonde, F., Murillo-Yarce, D., Guzman, J.I., Rivera, M.: Current control of the coupled-inductor buck-boost DC-DC switching converter using a model predictive control approach. *IEEE J. Emerg. Sel. Topics Power Electron.* 8(4), 3348–3360 (2020)
22. Kim, S.-K., Park, C.R., Kim, J.-S., Lee, Y.I.: A stabilizing model predictive controller for voltage regulation of a DC/DC boost converter. *IEEE Trans. Control Syst. Technol.* 22(5), 2016–2023 (2014)
23. Wang, B., Kanamarlapudi, V.R.K., Xian, L., Peng, X., Tan, K.T., So, P.L.: Model predictive voltage control for single-inductor multiple-output DC-DC converter with reduced cross regulation. *IEEE Trans. Ind. Electron.* 63(7), 4187–4197 (2016)
24. Li, X., Liu, Y., Xue, Y.: Four-switch buck-boost converter based on model predictive control with smooth mode transition capability. *IEEE Trans. Ind. Electron.* 68(10), 9058–9069 (2021)
25. Mohamed, E., Mohamed, A.: Adaptive model predictive control for DC-DC power converters with parameters' uncertainties. *IEEE Access* 9, 135121–135131 (2021)
26. Zhang, Q., Min, R., Tong, Q., Zou, X., Liu, Z., Shen, A.: Sensorless predictive current controlled DC-DC converter with a self-correction differential current observer. *IEEE Trans. Ind. Electron.* 61(12), 6747–6757 (2014)
27. Linares-Flores, J., Hernandez Mendez, A., Garcia-Rodriguez, C., Siramirez, H.: Robust nonlinear adaptive control of a “boost” converter via algebraic parameter identification. *IEEE Trans. Ind. Electron.* 61(8), 4105–4114 (2014)
28. Talbi, B., Krim, F., Laib, A., Sahli, A., Krama, A.: PI-MPC switching control for DC-DC boost converter using an adaptive sliding mode observer. In: Proceedings of 2020 International Conference on Electrical Engineering, pp. 1–5 (2020)
29. Wallscheid, O., Ngoumtsa, E.B.: Investigation of disturbance observers for model predictive current control in electric drives. *IEEE Trans. Power Electron.* 35(12), 13563–13572 (2020)
30. Xu, Q., Yan, Y., Zhang, C., Dragicevic, T., Blaabjerg, F.: An offset-free composite model predictive control strategy for DC/DC buck converter feeding constant power loads. *IEEE Trans. Power Electron.* 35(5), 5331–5342 (2020)
31. Wang, J., Tang, Y., Lin, P., Liu, X., Pou, J.: Deadbeat predictive current control for modular multilevel converters with enhanced steady-state performance and stability. *IEEE Trans. Power Electron.* 35(7), 6878–6894 (2020)

How to cite this article: Wu, Y., Wang, W., Tang, F., Wu, X., Chen, Z., Jing, L., Zhang, W.: Improved model predictive current control for multi-mode four-switch buck-boost converter considering parameter mismatch. *IET Power Electron.* 16, 1043–1062 (2023).
<https://doi.org/10.1049/pel2.12449>